

# Synchrosqueezed wavelet transform for frequency and damping identification from noisy signals

Luis A. Montejo\* and Aidcer L. Vidot-Vega

Department of Engineering Science and Materials, University of Puerto Rico at Mayagüez,  
Mayagüez, Puerto Rico

(Received September 29, 2011, Revised April 3, 2012, Accepted April 19, 2012)

**Abstract.** Identification of vibration parameters from the analysis of the dynamic response of a structure plays a key role in current health monitoring systems. This study evaluates the capabilities of the recently developed Synchrosqueezed Wavelet Transform (*SWT*) to extract instant frequencies and damping values from the simulated noise-contaminated response of a structure. Two approaches to estimate the modal damping ratio from the results of the *SWT* are presented. The results obtained are compared to other signal processing methods based on Continuous Wavelet (*CWT*) and Hilbert-Huang (*HHT*) transforms. It was found that the time-frequency representation obtained via *SWT* is sharpened than the obtained using just the *CWT* and it allows a more robust extraction of the individual modal responses than using the *HHT*. However, the identification of damping ratios is more stable when the *CWT* coefficients are employed.

**Keywords:** synchrosqueezing; reassignment; random decrement; wavelets; empirical mode decomposition; hilbert transform; fourier; time-frequency; damping; system identification

---

## 1. Introduction

Squeezing of the Continuous Wavelet Transform (*CWT*) was first introduced in the analysis of auditory signals for speaker identification (Daubuchies and Maes 1996) aiming to make the results of the *CWT* more robust to noise. The method was formally presented as the Synchrosqueezed Wavelet Transform (*SWT*) by Daubuchies *et al.* (2011), in this work the *SWT* was introduced as an alternative method to the Empirical Mode Decomposition (*EMD*) (Huang *et al.* 1998) to extract the oscillatory components of non-stationary signals. The *SWT* is a combination of wavelet analysis and a “reallocation” method (the synchrosqueezing) that concentrates the wavelet coefficients in the scale (frequency) dimension to sharpen the time - frequency representation of the signal, facilitating in this way the identification of ridges and extraction of components. While as original proposed, the *SWT* works based on the wavelet representation of the signal, it can be adapted to work on top of many invertible transforms like the Short Time Fourier Transform (Brevdo *et al.* 2011, Thakur and Wu 2010). Moreover, Li and Liang (2011) proposed a Generalized Synchrosqueezing Transform that reduce the spread of energy not only in the frequency but also in the time dimension and used the enhanced time frequency representation for gearbox fault diagnosis. Other successful implementations of synchrosqueezing have been reported in the analysis of biomedical and paleoclimate data

---

\*Corresponding author, Dr., E-mail: [luis.montejo@upr.edu](mailto:luis.montejo@upr.edu)

(Dabuchies *et al.* 2011, Chan *et al.* 2011, Brevdo *et al.* 2011), including the analysis of non-uniform samples (Thakur and Wu 2010).

In this study we use the original *SWT* method proposed by Daubuchies *et al.* (2011) through the fast implantation provided by Brevdo *et al.* (2011). Note that all of the previous applications of synchrosqueezing deal with the identification of instant frequencies and/or the extraction of mono-components. The objective of this work is to evaluate the capabilities of the *SWT* to identify damping ratios and instant frequencies from the simulated noise-contaminated response of a structure. Two approaches to estimate the modal damping ratio from the results of the *SWT* are presented. The results obtained are compared to other signal processing methods based on Continuous Wavelet (*CWT*) and Hilbert-Huang (*HHT*) transforms. Three different cases are evaluated: (1) the free response of a single degree of freedom (*dof*) system, (2) the free response of a 3-*dof* system with two closely spaced modes and (3) the forced response of a 3-*dof* system subjected to white noise base excitation. For each case different levels of noise are added to the simulated response to evaluate the detrimental effect of noise contamination in the different identification schemes.

Next we briefly described each of the methodologies being evaluated. The application of each method is exemplified using a *sdof* free decay response contaminated with different level of noise (case 1). Then we present the results obtained for the other two more challenging applications (case 2 and 3). For all the schemes evaluated, a portion of the signal is reflected at the beginning and the end in an effort to ameliorate end effects. Nevertheless, more elaborated procedures are available in the literature to overcome the edge-effect limitation (e.g., Boltežar and Slaviè 2004).

## 2. Hilbert transform and the analytic signal

The Hilbert Transform (*HT*) is named after the German scientist David Hilbert (Hilbert 1953, Johansson 1999) and is perhaps one of the easiest ways to compute the instant frequency and amplitude of a mono-component signal (i.e., a signal with only one frequency tone at any given time). The *HT* of a real valued function  $x(t)$  can be determined using Eq. (1) (Hahn 1996).

$$H[x(t)] = \frac{1}{\pi} \int_{-\infty}^{+\infty} \frac{x(\tau)}{t - \tau} d\tau \quad (1)$$

The *HT* is then the convolution integral of the function  $x(t)$  with the inverse of time  $1/t$ . With the *HT*, the Gabor analytic signal  $z(t)$  (Gabor 1946) of the function  $x(t)$  can be generated using Eq. (2) (Korpel 1982), where  $i$  denotes the imaginary unit.

$$z(t) = x(t) + iy(t) = x(t) + iH[x(t)] \quad (2)$$

The analytical signal  $z(t)$  is a two dimensional signal composed of a real part and an imaginary part. The Fourier transform of  $z(t)$  gives us a one-sided spectrum (the positive side) in the frequency domain. Eq. (2) can be re-written as

$$z(t) = a(t)e^{i\theta(t)} \quad (3)$$

where

$$a(t) = \sqrt{x^2 + y^2} \quad \text{and} \quad \theta(t) = \arctan\left(\frac{y}{x}\right) \quad (4)$$

This means that the analytic signal allow us to decompose a signal in their instant amplitude  $a(t)$  and instant phase  $\theta(t)$  components. Starting from Eq. (3), Ville (1948) proposed the concept of instant frequency ( $IF$ ) as the time derivative of the phase

$$IF(t) = \frac{1}{2\pi} \frac{d}{dt} \theta(t) \tag{5}$$

Direct application of Eqs. (1)-(5) to obtain the instant frequency of a signal will give us an  $IF$  function with discontinuities every time the phase reach values of  $\pi$  or  $-\pi$  due to the use of the arctan function in the calculation of the phase. To solve this problem the phase can be unwrapped (i.e., add  $2\pi$  each time a cycle is completed) before it is used to calculate the  $IF$ . Alternatively one can take the phase of the derivative instead of the derivative of the phases (Feldman 2011)

$$IF_n = \frac{1}{2\pi} \arctan(z_n \text{conj}(z_{n+1})) \tag{6}$$

In the case of the free vibrations of a sdof the response of the system can be expressed as

$$D = Ae^{-\zeta\omega_n t} \cos(\omega_d t - \alpha) \tag{7}$$

where  $\omega_n$  is the system's natural frequency (in rad/s),  $\omega_d$  is the damped natural frequency and  $\zeta$  is the damping ratio. Therefore, the  $IF$  values obtained from the analysis of the free vibration decay correspond to the damped frequency of the system. By comparison with Eq. (3), the calculated instant amplitude  $a(t)$  will correspond to the envelope of the decay ( $Ae^{-\zeta\omega_n t}$ ). If the function  $a(t)$  is linearized by taking the natural logarithm, the slope of the resultant line will be equal to  $\zeta\omega_n$  and the system's damping ratio and natural frequency can be calculated using Eqs. (8) and (9) respectively.

$$\zeta = \frac{(\zeta\omega)^2}{\omega_d^2 + (\zeta\omega_n)^2} \tag{8}$$

$$\omega_n = \frac{\omega_d}{\sqrt{1-\zeta^2}} \tag{9}$$

A numerical implementation of the  $HT$  for system identification is presented next. Fig. 1 shows

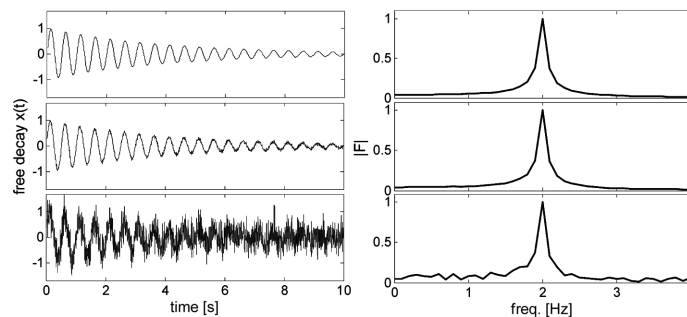


Fig. 1 Free decay response of a damped  $SDOF$  system (Left) with different level of noise added and its Fourier spectrum (Right): response without noise (top), response with  $SNR=10$  (middle) response with  $SNR=1$  (bottom)

10 seconds of free decay response (Eq. (7)) of a s dof with natural frequency 2 Hz and damping ratio 2% (sampling frequency was 200 Hz). To account for the detrimental effect of noise contamination expected in any practical implementation, different levels of white noise were added to the simulated response. The signal-to-noise ratio ( $SNR$ ) for each case was defined as

$$SNR = \frac{\sigma_x}{\sigma_n} \quad (10)$$

where  $\sigma_x$  is the standard deviation of the signal and  $\sigma_n$  is the standard deviation of the additive white noise. In addition to the noise-free case, 10 other cases were analyzed, ranging from low noise levels ( $SNR=10$ ) to the noise embedded case ( $SNR=1$ ). Fig. 1 also shows the Fourier spectra of the response, it is seen that even in the critical case ( $SNR=1$ ), the frequency of the system can be identified from the Fourier spectrum.

The results of applying the  $HT$  to the signals without noise and with  $SNR=1$  is presented in Fig. 2. It is seen that the results obtained for the signal without noise are stable and allow the identification of the system's frequency and damping. However, for the signal with  $SNR=1$  it is seen that identification of the system frequency is not possible due to the scatter in the results. The results obtained for the linearized instant amplitude also present some important dispersion but still permit the fitting of a line. The results for the damping ratios estimated for each case are summarized in Fig. 8 (circular markers -  $HT$ ). Since identification of the system frequency was not possible for the signals with a high level of noise, the damping values were extracted from the slope of the line fitting the instant amplitude using the frequency identified via Fourier spectrum (2 Hz). Notice also that to avoid end effects the first and last 2 seconds of the response were omitted in the fitting. The results presented in Fig. 8 show that the errors in the estimation of the damping ratios is maintained below 5% until  $SNR=5$ , from this point the error start increasing faster until reaching more than 60% at  $SNR=1$ . Due to its sensitivity to noise,  $HT$  identification methods require high quality experimental measurements with a minimum of instrumental noise (Feldman 2011b).

### 2.1 Hilbert-Huang transform

In addition to its sensitivity to noise, the other great challenge that faces the  $HT$  is its limitation to mono-component signals. When the  $HT$  is applied to a multi-component signal (i.e., a signal in which more than one frequency is present at a given time) the result obtained for the instant frequency at a

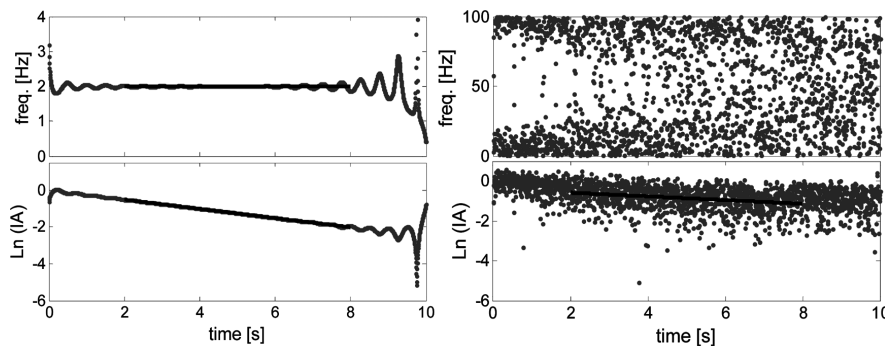


Fig. 2 Calculation of instant frequency and damping via Hilbert transform of the response without noise (left) and with  $SNR=1$  (right)

specific time will be the average of the frequencies occurring at that time. Therefore, in order to analyze a multi-component signal with the *HT*, the signal is first decomposed into its mono-components constituents. Several methodologies like the Empirical Mode Decomposition (Huang *et al.* 1998), the Hilbert Vibration Decomposition (Feldman 2006) or the use band-pass filters have been proposed to accomplish this purpose. In this work we use the Empirical Mode Decomposition (*EMD*) algorithm to pre-process the signal and then apply the *HT* to each component (or the component of interest). This procedure of applying the *EMD* and then the *HT* individually to the mono-components (or Intrinsic Mode Functions *IMFs*, as called by Huang) is known as the Hilbert-Huang Transform (*HHT*).

The *EMD* is an iterative sifting algorithm where the signal is decomposed into *IMFs* and a residue. These *IMFs* are defined so as to ensure that they have well-behaved HTs and conform to a narrowband condition. An *IMF* represents a simple oscillatory mode as a counterpart to the simple harmonic function, but it is much more general: instead of having a constant amplitude and frequency, as in a simple harmonic component, the *IMF* can have a variable amplitude and frequency as function of time (Huang 2005). The *EMD* was implemented in this work by means of the algorithm provided by Rilling *et al.* (2003). Fig. 3 show the results obtained via *HHT* for the sdof free decay with *SNR*=1. A total of 8 *IMFs* were obtained with the first 5 *IMFs* (not shown) containing most of the noise added to the signal. Although most of the noise was isolated we cannot say that the decomposition was completely successful as the vibration mode was captured in three different *IMFs* (6, 7 and 8) instead of one. This phenomenon is common when analyzing signals with a high level of noise and is known as mode mixing. We tried using more rigorous parameters for the *EMD* algorithm and using an ensemble of *EMD* results from different noise added signals (*EEMD*, Wu and Huang 2009) obtaining no significant improvements. The vibration mode was then reconstructed by adding *IMFs* 6 to 8. When the *HT* is applied to the reconstructed signal, the dispersion in the resulting *IF* values is improved when compared to the *HT* alone results (Fig. 2), but still do not allow a robust estimation of the frequency. However, the instant amplitude results are more stable and permit the fitting of a line. As for the *HT* case in the previous section, the value of the damping ratio was extracted using the frequency identified by the Fourier spectrum (2 Hz). A summary of the errors in the estimation of the damping ratios is presented in Fig. 8 (square markers - *EMD+HT*). It is seen that the results are significantly improved specially for the signals with a high level of noise contamination, for example for the *SNR*=1 case, the error is maintained below 15% while for the *HT* approach the error was above 60%.

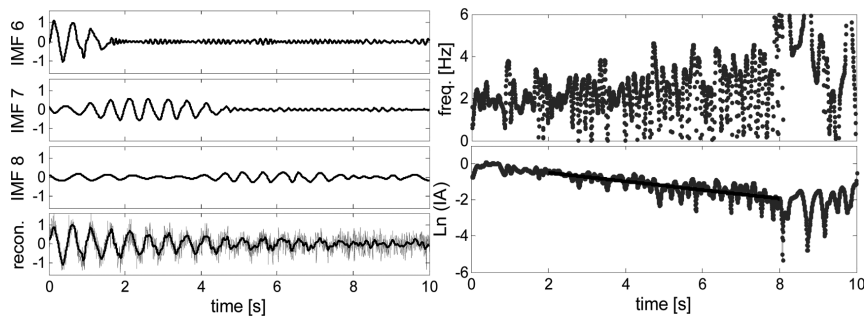


Fig. 3. *HHT* results for the signal with *SNR*=1. Left: *IMFs* 6, 7 and 8 obtained via *EMD* and the reconstructed signal along with the original signal. Right: Calculation of instant frequency (top) and damping (bottom) via Hilbert transform of the component extracted via *EMD*

### 3. Continuous wavelet transform

The wavelet transform is a two-parameter transform: for a time signal  $x(t)$ , the two transformed domains are time  $b$  and scale  $a$ . The scale  $a$  is inversely proportional to a frequency that depends on the type of wavelet used. The Continuous Wavelet Transform (*CWT*) of a signal  $x(t)$  is defined by the integral

$$W(a,b) = \int_{-\infty}^{\infty} x(t)\psi_{a,b}(t)dt \quad (11)$$

The function  $\psi_{a,b}(t)$  in Eq. (11) is referred to as the wavelet function. It is defined by translating along the time axis and stretching the mother wavelet  $\Psi(t)$

$$\psi_{a,b}(t) = \frac{1}{\sqrt{a}}\Psi\left(\frac{t-b}{a}\right) \quad (12)$$

The wavelet coefficients  $W(a,b)$  contain information about the function  $x(t)$  at the scale  $a$  around the time position  $b$ . The selection of the proper mother wavelet is crucial for the successful implementation of a given application. For this work we choose the Complex Morlet Wavelet (Grossman and Morlet 1990) as it has been successfully used in the past for system identification purposes (e.g., Todorovska 2001, Kijewski and Kareem 2003, Montejo and Suarez 2006). The wavelet coefficients  $W(a,b)$  resulting from applying the *CWT* along with the Morlet wavelet with a central frequency of 1 Hz to the sdof response embedded in noise (Fig. 1,  $SNR=1$ ) are shown in its absolute values in the Wavelet Map displayed in Fig. 4 (left). The darker colors indicate higher values of the wavelet coefficients. Since the wavelet coefficients take on maximum values at the instantaneous frequency (Carmona *et al.* 1997), by observing the dark trends in the graph one can detect the dominant frequencies in the signal. These trends define ridges in the time-frequency plane. Extracting the values of the wavelet coefficients along each ridge yields a wavelet skeleton, which real and imaginary components are directly proportional to the signal content at that frequency and its corresponding *HT* (Staszewski 1997, Kijewski and Kareem 2003). The wavelet coefficients along the ridges can then be used to form the analytic signal (Eq. (3)) for each component, allowing the identification of instant frequencies and damping ratios. The ridges can be extracted by a variety of techniques (e.g., Carmona *et al.* 1997); in this work we used the algorithm available from the Synchronsqueezing Toolbox (Brevdo *et al.* 2011). This is a dynamic algorithm that maximizes a

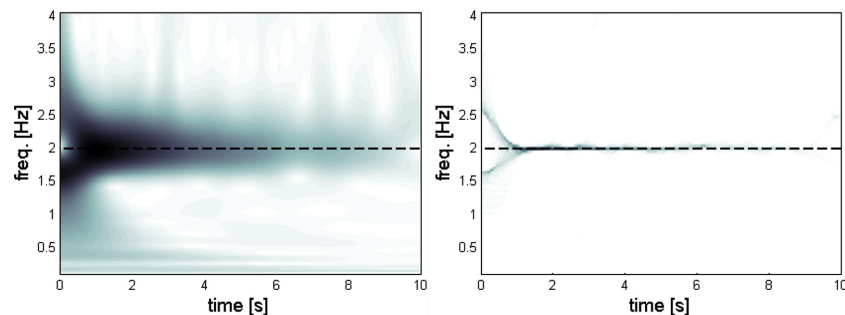


Fig. 4 Wavelet Transform (left) and Synchronsqueezed Wavelet Transform (right) along with the *IF* curves extracted (dashed lines) of the response with  $SNR=1$

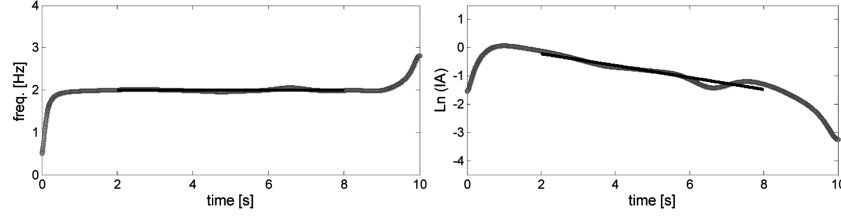


Fig. 5 Frequency (left) and damping (right) calculation for the response with  $SNR=1$  using the ridge coefficients  $CWT$  to define the analytic signal

functional of the energy of the curve being extracted that penalizes variation. There is a user-defined parameter ( $\lambda > 0$ ) that determines the “smoothness” of the resulting curve estimate, we used  $\lambda=10^6$  for all the examples in this work. The extracted ridge is shown in Fig. 4 (left - dashed line). The frequency and damping ratio results based on the wavelets coefficients along the ridge are shown in Fig. 5. It is seen that the resulting representation for the instant frequency and amplitude are more stable than the obtained with the  $HT$  and  $HHT$  approaches (Figs. 2 and 3, respectively). Fig. 8 presents the error in the damping ratio estimate for all the different levels of noise contamination (left pointing triangle markers -  $WT$  coeff.), it is seen that in general this approach provides lowest errors than the  $HT$  and  $HHT$  approaches.

### 3.1 Synchrosqueezed wavelet transform

The Synchrosqueezed Wavelet Transform ( $SWT$ ) is a novel adaptive time-frequency analysis technique first introduced in context of speaker identification (Daubuchies and Maes 1996) and further developed in Daubuchies *et al.* (2011). The  $SWT$  is a relocation-type transform aimed to sharpen the time frequency representation of a signal by “concentrating” the wavelet coefficients in the scale (frequency) dimension. In contrast to the reallocation methods discussed in Auger and Flandrin (1995) and Chassande-Mottin *et al.* (1997, 2003), synchrosqueezing is adaptive to the given signal, i.e., independent of the particular window function used, and allows the signal to be reconstructed from the reallocated coefficients (Thakur and Wu 2010, Wu 2011). The  $SWT$  consists of three steps:

- (1) Compute the  $CWT$  coefficients (Eqs. (11)-(12))
- (2) Perform an initial estimate of the instantaneous angular frequency  $\omega(a,b)$  at any  $(a,b)$  location where  $W(a,b) \neq 0$  using Eq. (13)

$$\omega(a,b) = \frac{-i}{W(a,b)} \frac{\partial}{\partial b} W(a,b) \quad (13)$$

(3) The wavelet coefficients  $W(a,b)$  are squeezed via reassignment based on  $\omega(a,b)$  to generate the Synchrosqueezed representation  $T(\omega,b)$ . In practical applications the wavelet coefficients are computed only at discrete scales  $a_k$  and its Synchrosqueezed transform is determined at the centers of the bins  $[\omega_c - \Delta\omega/2, \omega_c + \Delta\omega/2]$

$$T(\omega_c, b) = \frac{1}{\Delta\omega} \sum_{a_k: |\omega(a_k, b) - \omega_c| \leq \frac{\Delta\omega}{2}} W(a_k, b) a_k^{-3/2} (\Delta a)_k \quad (14)$$

where  $(\Delta a)_k = a_k - a_{k-1}$  and  $\Delta\omega = \omega_c - \omega_{c-1}$ . The detailed derivation Eqs. (13) and (14) is presented in

Daubuchies *et al.* (2011). In this work the *SWT* was performed using the fast implementation provided by Brevdo *et al.* 2011, which computes the Discrete Wavelet Transform (*DWT*) using the Fast Fourier Transform (*FFT*) and optimize the discretization of the squeezing operator  $T$ . The *DWT* samples the wavelet coefficients at scale locations  $a_j = 2^{j/nv} \Delta t$  where the number of voices ( $nv$ ) defines the frequency resolution of the analysis, we used  $nv=32$  in all of the applications presented in this work.

The result obtained from applying the *SWT* to the *sdof* response embedded in noise (Fig. 1,  $SNR=1$ ) is shown in Fig. 4 (right) along with the extracted ridge (dashed line). When compared to the Wavelet Map (Fig. 4-left) it is seen that through the *SWT* we obtained a sharper, easier to interpret time-frequency representation of the signal. This permits a well-defined identification and extraction of the ridges, allowing further reconstruction of the independent components of the signal. Notice that with the wavelet transform, the signal  $x(t)$  can be retrieved from the wavelet coefficients  $W(a,b)$  with the so-called “reconstruction formula” (Grossman and Morlet 1984)

$$x(t) = \frac{1}{K_\psi} \int_{a=0}^{\infty} \int_{b=-\infty}^{\infty} C(a,b) \psi_{a,b}(t) \frac{db}{a^2} da \quad (15)$$

where  $K_\psi$  is a constant that depends on the mother wavelet. One can use Eq. (15) to extract the independent components of the signal by integrating over a subregion of the integrating domain along the identified ridge  $c$ . The integration is then restricted to the scale/frequency window  $[c-n_w, c+n_w]$ , for this example we used  $n_w=4$ . However and as other authors have noticed (Daubuchies *et al.* 2011, Brevdo *et al.* 2011), the *SWT* time-frequency representation is very concentrated, so that the width of the integration window does not affect much the final result (unless the signal has components with closely separated frequencies, in which case care must be taken not to interfere with each other). Once the component is extracted, the subregion used is subtracted from the *SWT* representation by setting  $T(a,b)=0$  in that region. Next, one can search for the next ridge and its associate component (if dealing with multicomponent signals) or reconstruct the residual signal from the remaining coefficients (which is usually associated with the noise in the signal). Fig. 6 (left) shows the component and residue extracted for the *sdof* free decay with  $SNR=1$ . It is seen that the results obtained are more robust than the obtained via *EMD* (Fig. 3 left) as the response of the *sdof* is completely captured in a single component avoiding the need for further analysis and re-assembling of components. Once the components are extracted, the *HT* approach previously described can be used to construct the analytic signal and obtain estimates for the instant frequency and damping in the system. The results obtained are displayed in

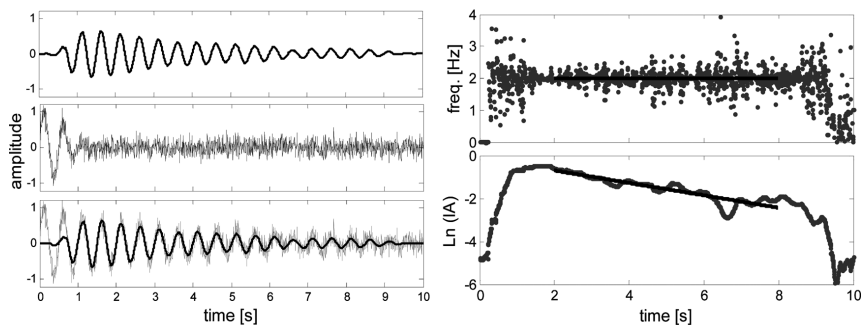


Fig. 6 Left: Component extracted via *SWT* (top) of the response with  $SNR=1$ , residue (middle) and original signal (gray line) along with the component extracted (black line) via *SWT* (bottom). Right: Calculation of instant frequency (top) and damping (bottom) via Hilbert transform of the component extracted via *SWT*

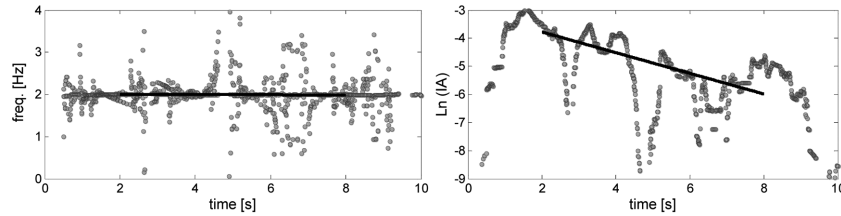


Fig. 7 Frequency (left) and damping (right) calculation for the response with  $SNR=1$  using the ridge coefficients of the *SWT* (top) and *CWT* (bottom) to define the analytic signal

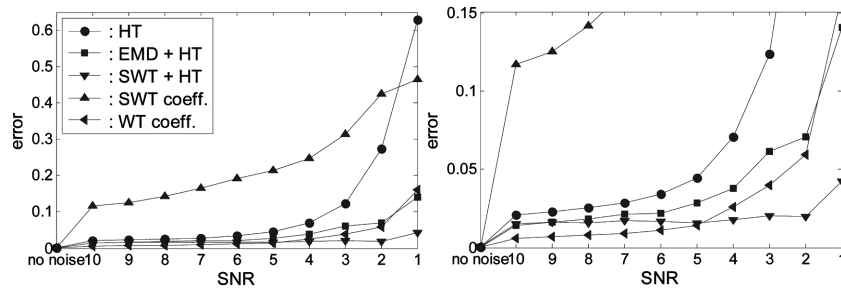


Fig. 8 Error in the estimation of damping from signals with different levels of noise, right figure is a zoom-in of the figure on the left

Fig. 6 (right), it is seen that the *HT* of the component extracted via *SWT* behave better than the *HT* of the component extracted via *EMD* (Fig. 3 right) allowing a more robust estimation of the system frequency and damping. The results obtained for all the levels of noise contamination are summarized in Fig. 8 (triangular marker facing down - *SWT+HT*). For high levels of noise contamination ( $SNR$  4 to 1) the computed errors are the lowest of all the methods evaluated, staying below 5% even in the noise embedded case.

Alternatively one can proceed as with the wavelet coefficients, i.e., using the real and imaginary parts of the coefficients along the ridge to build the analytic signal. It is seen from the results displayed in Fig. 7 that, at least for this particular case, the instant frequency and instant amplitude results are more disperse than the obtained using the *HT* of the component extracted via *SWT* (Fig. 6). When compared to the other evaluated methodologies along the different levels of noise contamination (Fig. 8) this method exhibits the largest errors.

### 3.2 Free decay of a 3-dof system with two closely spaced modes

This example is taken from Yan and Miyamoto (2006) and is used to compare the capabilities of the different signal processing based system identification methodologies when the structure exhibits modes with frequencies closely spaced. The natural frequencies of the system are 1 Hz, 1.06 Hz and 2 Hz, the damping ratio for the three modes is 1% and the sampling frequency is 20 Hz. The free decay response of the system with different levels of noise contamination is displayed in Fig. 9 along with its Fourier spectrum. It is seen that for low levels of noise contamination the three natural frequencies of the system can be clearly identified from the Fourier spectrum. However, identification of the third mode frequency (2 Hz) is compromised in the noise embedded case ( $SNR=1$ ) due to presence of additional peaks of comparable amplitude in the vicinity. Since the signal being analyzed is

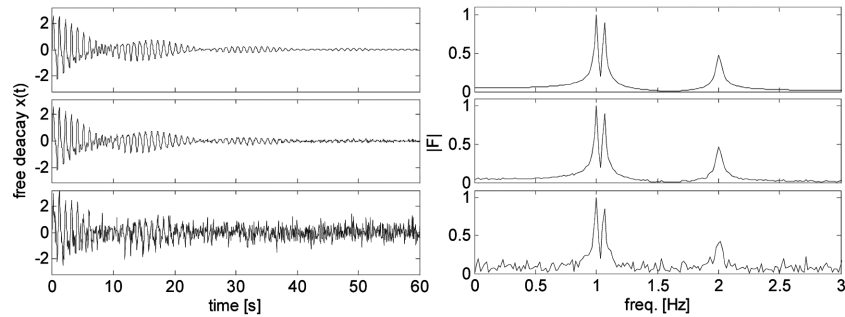


Fig. 9 Free decay response of a damped 3 *DOF* system with different levels of noise added (Left) and its Fourier spectrum (Right): response without noise (top), response with  $SNR=10$  (middle) response with  $SNR=1$  (bottom)

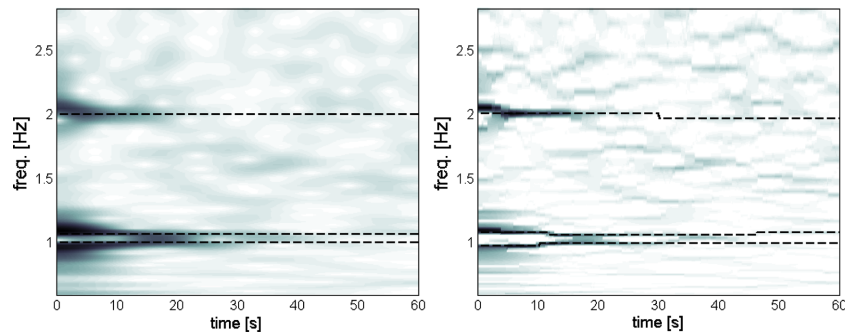


Fig. 10 Wavelet Transform (left) and Synchrosqueezed Wavelet Transform (right) along with the IF curves extracted (dashed lines) of the response with  $SNR=1$

comprised of three modal responses, an analysis based on the direct application of the *HT* is not appropriate and preprocessing of the signal is required to extract the independent components (modal responses). Application of the *EMD* and *EEMD* methodologies to extract the modal responses failed to separate the two closely spaced modes; same results were reported by Yan and Miyamoto (2006) using *EMD* and band-pass filtering.

The time-frequency representations of the signal with  $SNR=1$  via *CWT* and *SWT* are presented in Fig. 10 along with the identified ridges. The results presented were obtained using the Complex Morlet Wavelet with a central frequency of 6 Hz to allow separation of the closely spaced modes. Further details on the identification of closely spaced modes and close modes cross talk arising from the frequency spread of the Continuous Wavelet Transform is available elsewhere (e.g., Kijewski and Kareem 2003, Slaviè *et al.* 2003, Chen *et al.* 2009). To define the integration window width we use  $n_w=2$  for the *CWT* representation and  $n_w=1$  for the *SWT* representation. The components extracted via *SWT* for the  $SNR=10$  and  $SNR=1$  signals are presented in Fig. 11 (black lines) along with the theoretical modal responses (gray lines). The detrimental effect of noise contamination is clearly appreciated from the results obtained, it is seen that the poorest results are obtained for the identification of the third mode after 30 seconds in the noise embedded case. This confirms the demonstrated theoretically in Brevdo *et al.* (2011): in noise contaminated signals, reconstruction of the signal components is less reliable in locations of high frequencies and low magnitudes. The determination of damping ratios is performed using three approaches: (1) *HT* of the components extracted via

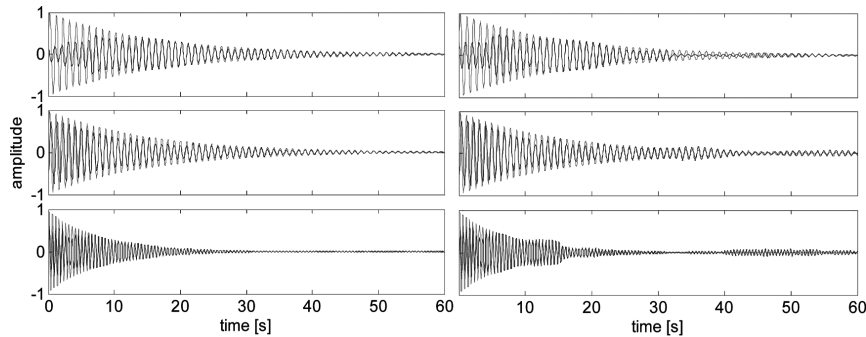


Fig. 11 Components extracted via *SWT* (black line) and target function (gray line): signal with  $SNR=10$  (left) and  $SNR=1$  (right)

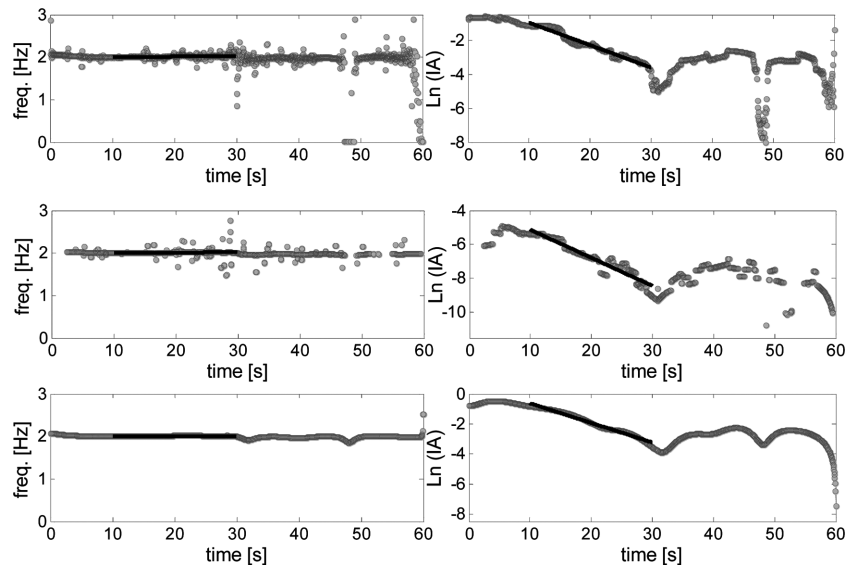


Fig. 12 Instant frequency (left) and damping calculation (right) from the 2.00 Hz mode of the response with  $SNR=1$ , from top to bottom: *SWT+HT*, *SWT* coefficients and *CWT* coefficients

*SWT* (*SWT+HT*), (2) construction of the analytic signal from the *SWT* coefficients along the ridges (*SWT coeff.*) and (3) construction of the analytic signal from the *CWT* coefficients along the ridges (*WT coeff.*). Fig. 12 shows the results obtained for the critical case (i.e., identification of the 2 Hz mode using the signal with  $SNR=1$ ), the fitting was limited to the range 10-30 seconds, after this time the instant amplitude results obtained were not reliable in all three methodologies. Notice that the added noise was of constant amplitude and the original signal a free-decay. Therefore, the resulting contaminated signal does not have a constant  $SNR$  value but it is rather increasing with time. The reported  $SNR$  values can be seen as an average value over the whole signal. Taking this into account and the fact that high frequencies damp faster than low frequencies (see Fig. 11 left), it can be said that for this specific scenario the  $SNR$  after 30 seconds is well below 1. While not really required for all the  $SNR$  cases and vibration modes, for comparison purposes the range [10-30] seconds was used in all cases for the fitting of the instant amplitude. Fig. 13 presents a summary of the results obtained, since the results obtained vary largely between modes and noise level, it is difficult to point out a

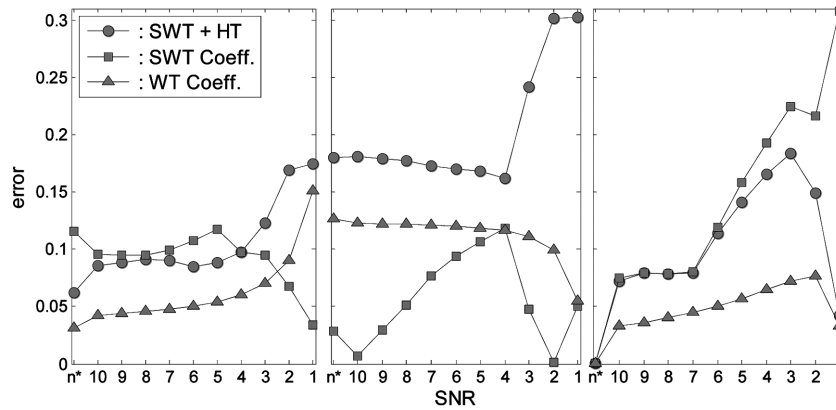


Fig. 13 Error in the estimation of damping from signals with different levels of noise ( $n^*$ =no noise): 1.06 Hz mode (left), 1.00 Hz mode (middle) and 2.00 Hz mode (right)

specific method as the “best one.” However, it can be said that the more stable results are obtained using the wavelet coefficients along the ridge, through this method the error was maintained always below 13% and the results do not exhibit sudden changes as for the other two methodologies. This is reinforced by looking back at Fig. 12 and noticing that the *CWT* results offer the lower dispersion in the instant frequency and instant amplitude plots.

### 3.3 3-dof system subjected to white noise base excitation

Evaluation of the identification methodologies when the structure is under forced vibrations is performed using a three story linear shear building model subjected to 160 seconds of white noise base excitation. The specified properties were  $m_1=m_2=m_3=300$  kg and  $k_1=k_2=k_3=100000$  N/m. The system natural frequencies are 1.29, 3.62, and 5.24 Hz; a damping ratio of 2% was specified for the three modes. Sampling frequency was 100 Hz. In the sake of brevity we analyzed only the response of the system that would be registered by an accelerometer located in the top floor. This response with different levels of noise contamination is displayed in Fig. 14 along with their Fourier spectra. Due to the location of the sensor and the geometry of the modes, it is seen that the first mode (1.29

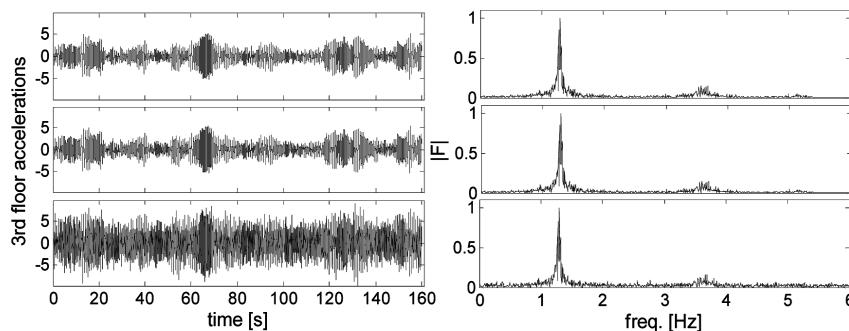


Fig. 14 Acceleration response of a 3 *DOF* system subjected to white noise excitation at its base with different level of noise added (Left) and its Fourier spectrum (Right): response without noise (top), response with  $SNR=10$  (middle) response with  $SNR=1$  (bottom)

Hz) basically dominates the response. The second (3.62 Hz) and third mode (5.24 Hz) can be somehow identified from the Fourier spectrum when the noise level is low. However, for the noise embedded case the third mode is no longer identifiable and the second mode got blurred by the presence of additional peaks in the vicinity.

Notice that for the other two examples the free decay response was given; in this case the available signal is the response of the system to a random excitation. Extraction of the decay curves can be accomplished by means of the Random Decrement Technique *RDT* (e.g., Kijewski and Kareem 2003, Yang *et al.* 2004). The *RDT* was developed by Cole (1968) in the context of damage detection of aerospace structures and have widely used since then in other applications. The *RDT* assumes that the random response of a damped structure is composed of a deterministic part and a random part. By averaging enough segments of the same random response, the random part will average out leaving the deterministic part, which is proportional to the free decay (Al-Sanad *et al.* 1983).

Two different approaches were examined: (1) Extract the modal responses via *HHT* or *SWT* and then applied the *RDT* to the extracted components and (2) Apply first the *RDT* technique to the original signal and then apply the *HT*, *CWT* or *SWT* to the extracted random signature (*RS*). Fig. 15 show the results obtained from the application of the *HHT* to the response without noise, it is seen from the instant frequency plot that this methodology failed to completely separate the modal responses. The results obtained via *SWT* are displayed in Fig. 16 for the two extreme cases, the response without noise and the response embedded in noise. For both cases the *SWT* identified the frequencies for the first two modes only. As discussed earlier, this is in large part due to the location of the sensor, top floor, where the contribution of the third mode is minimal. Once the components are extracted

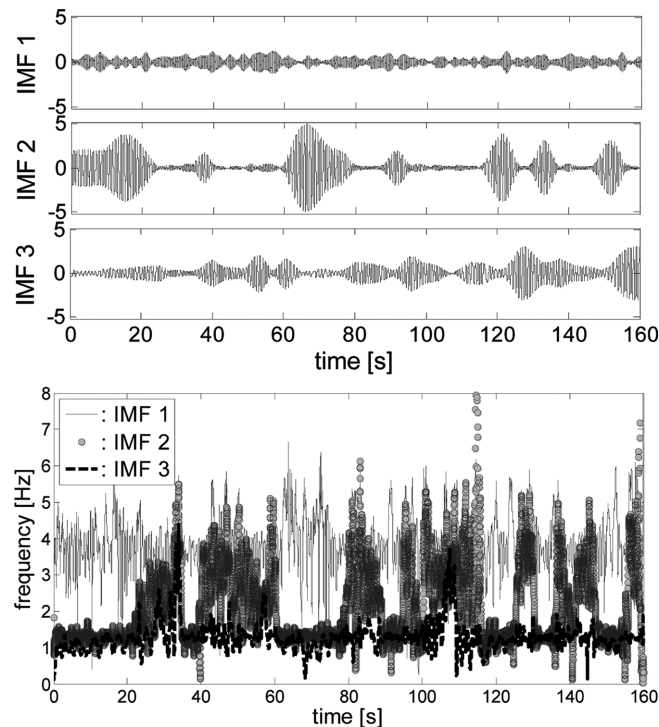


Fig. 15 First three *IMFs* of the response without noise obtained via *EMD* (top) and their instant frequency via *HT* (bottom)

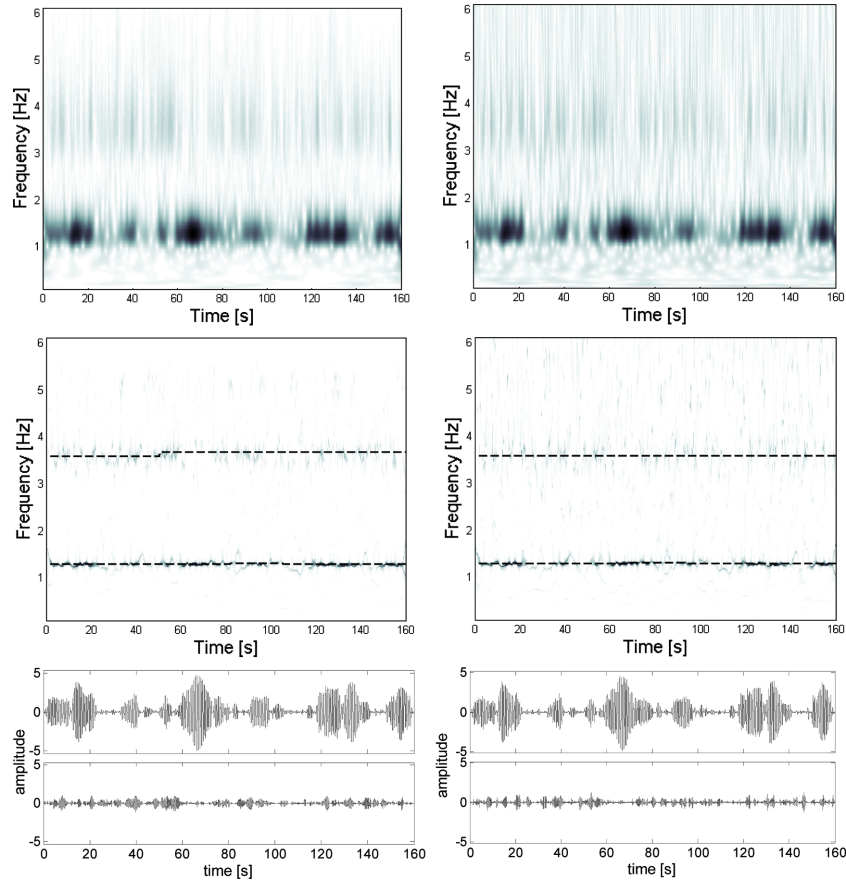


Fig. 16 Extraction of components via *SWT* of the response without added noise (left figures) and with  $SNR=1$  (right figures). Top: Wavelet Map, middle: *SWT* Map with identified ridges, bottom: extracted components

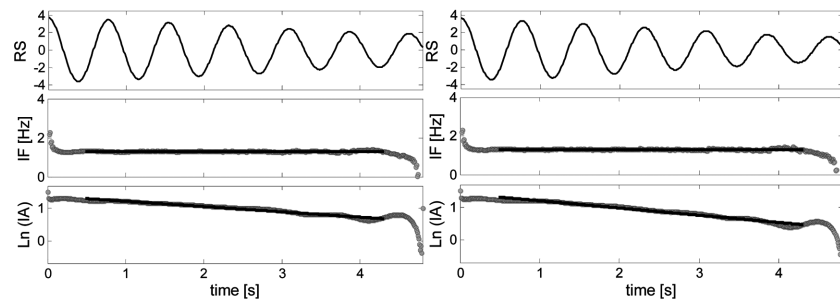


Fig. 17 Random signatures (*RS*) extracted from the *SWT* first component with their instant frequencies (*IF*) and instant amplitudes (*IA*). Left: results for the response without added noise, right: results for the response with  $SNR=1$

the *RDT* is applied to each of them to obtain the *RS* (i.e., the free decay) and the damping and frequency are obtained via *HT* of the free decay. The results obtained for the first mode (1.29 Hz) and the second mode (3.62 Hz) are presented in Figs. 17 and 18, respectively. It is seen that more stable (less dispersion) plots are obtained for the first mode. This was expected since this is the mode

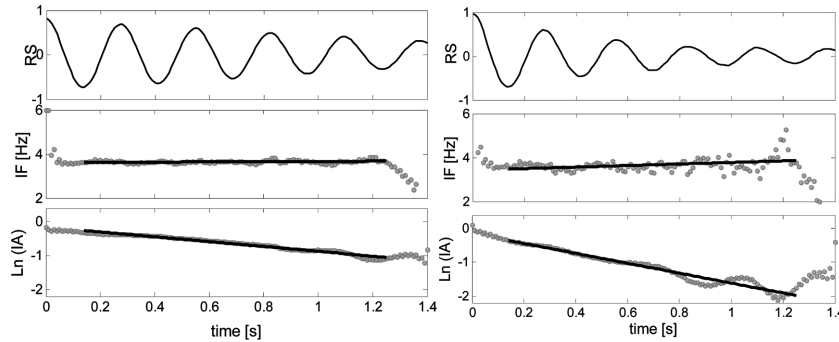


Fig. 18 Random signatures (*RS*) extracted from the *SWT* second component with their instant frequencies (*IF*) and instant amplitudes (*IA*). Left: results for the response without added noise, right: results for the response with  $SNR=1$

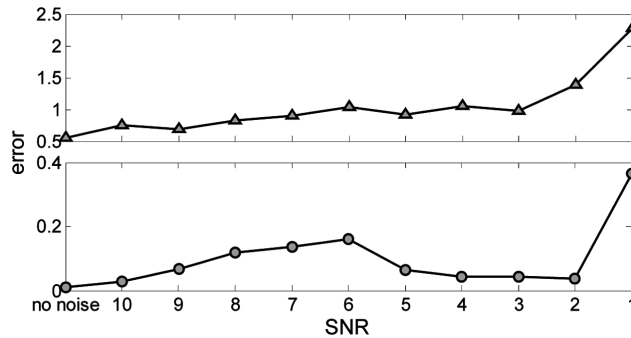


Fig. 19 Error in the estimation of damping from signals with different levels of noise: 1.29 Hz mode (bottom) and 3.62 Hz mode (top)

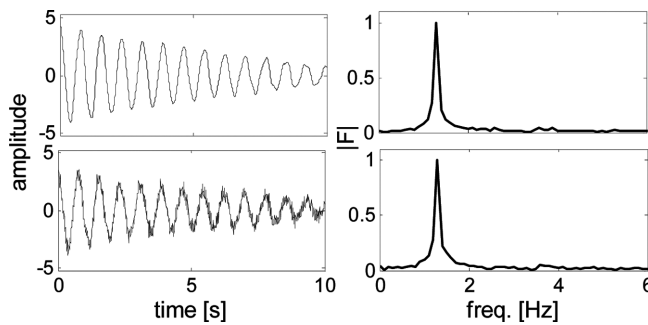


Fig. 20 Random signatures extracted for the 3<sup>rd</sup> floor acceleration response (left) and their Fourier spectrum (right). Top: results for the response without added noise, bottom: results for the response with  $SNR=1$

dominating the response in the third floor, as can be inferred from the Fourier spectra (Fig. 14) and Wavelet Maps (Fig. 16), most of the energy in the signal arises from this mode. A summary of the errors in the estimated damping values for both modes and using different levels of noise contamination is presented in Fig. 19. As expected, better results are obtained for the first mode where the errors were maintained below 20% with exception of the noise embedded case. On the other hand, the results obtained for the second mode are very poor, with errors ranging from 50% to

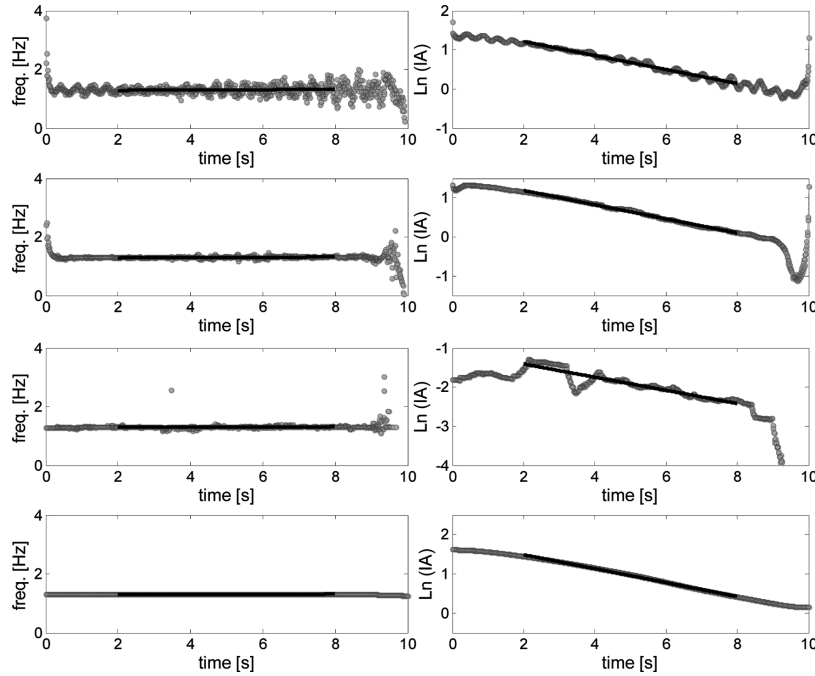


Fig. 21 Instant frequency (left) and damping calculation (right) from the analysis of the random signature of the response with  $SNR=10$ , from top to bottom: direct application of Hilbert Transform ( $HT$ ) to random signature,  $SWT+HT$ ,  $SWT$  coefficients and  $CWT$  coefficients

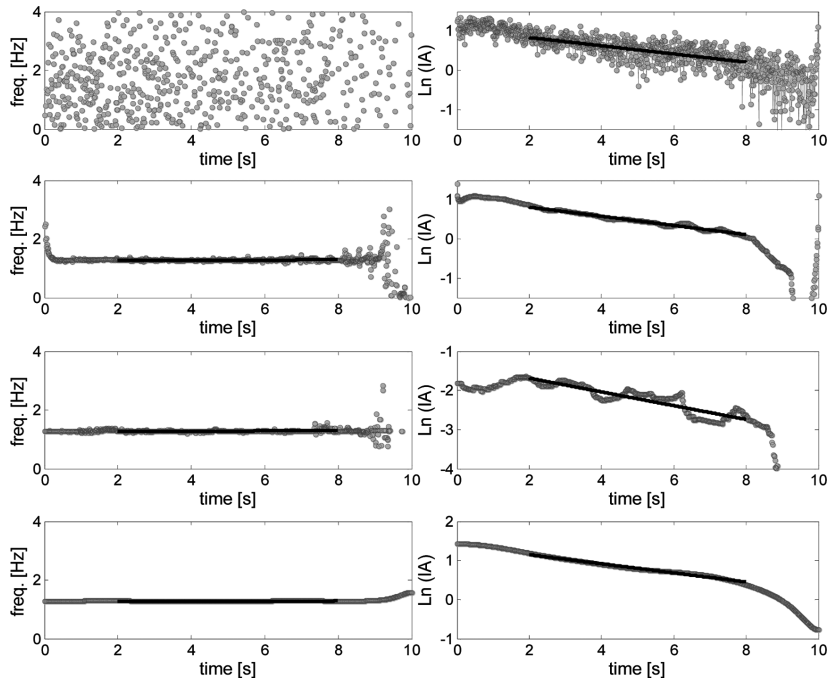


Fig. 22 Instant frequency (left) and damping calculation (right) from the analysis of the random signature of the response with  $SNR=1$ , from top to bottom: direct application of Hilbert Transform ( $HT$ ) to random signature,  $SWT+HT$ ,  $SWT$  coefficients and  $CWT$  coefficients

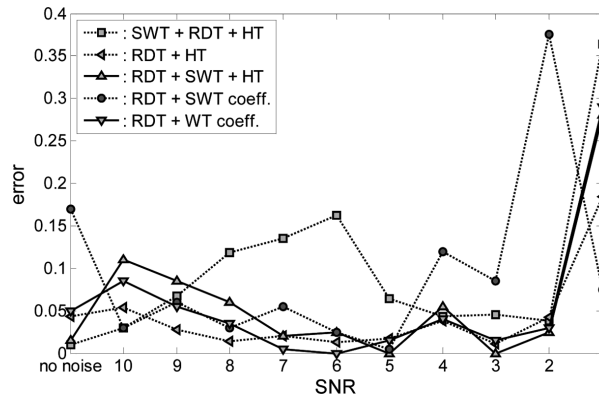


Fig. 23 Error in the estimation of damping from signals with different levels of noise

more than 200%.

The second approach consisted of applying the *RDT* directly to the response of the structure and then the other signal processing approaches are applied to the extracted signature for identification purposes. The extracted *RS* from the response without noise and with *SNR*=1 are presented in Fig. 20 along with their Fourier spectra. It is seen that the “averaging” process has basically wiped out the second mode. Therefore, the identification process was only possible for the first mode. The instant frequency and instant amplitude plots resulting from the application of the *HT*, *SWT+HT*, *SWT* coeff. and *CWT* coeff. approaches to the extracted *RS* are presented in Fig. 21 for the signal with *SNR*=10 and in Fig. 22 for the signal with *SNR*=1. It is seen that for the case with low noise contamination a direct application of the *HT* to the *RS* may be enough. However, for larger levels of noise contamination a more advanced processing of the *RS* is required. Fig. 23 summarizes the results of all the methodologies examined for this application, based on the results presented in this figure and the behavior observed in Figs. 21 and 22, it can be said that the more stable results are obtained when the wavelet coefficients from the ridge of the *RS* are used to build the analytic signal (*RDT + WT coeff.*).

#### 4. Conclusions

In this paper we examined the capabilities of the novel *SWT* to identify natural frequencies of vibration and damping ratios from structural responses of different nature and contaminated with different levels of noise. In addition to the *SWT*, other signal processing based identification techniques based on Hilbert-Huang and Continuous Wavelet transforms were evaluated. It was found that through the *SWT* a crisper time-frequency representation of the signal is obtained. This enables an unambiguous identification and extraction of the instant frequency ridges, allowing further reconstruction of the independent components of the signal and offering an alternative to the popular *EMD* methodology. In the *EMD* approach the signal individual components are obtained as an intermediary result which is later used to obtain the instantaneous frequency and amplitude profiles via *HT*. With the *SWT*, the independent components are obtained in an additional step after the frequency profiles are extracted. In the applications presented, it was found that the *SWT* allows a more robust extraction of the individual components than the *HHT*. However, the results obtained also show that the generation of

instant amplitude plots (used to determine the damping ratios) is more stable when the wavelet coefficients along the identified ridges is used to build the analytic signal. Future research efforts may focus on the advantages of using the *SWT* in other areas where the *CWT* has already demonstrated its convenience, like damage detection techniques (e.g., Gokdag and Kopmaz 2010, Montejo 2011) and soil-structure interaction problems (Bagheripour *et al.* 2010).

## Acknowledgements

This research is supported by the National Science Foundation Grant No. CMMI-1121146. The authors would like to thank Dr. E. Brevdo, Dr. J. Lu and Professor P. Flandrin for making publicly available their codes for the Synchrosqueezing, ridge extraction and *EMD* implementations, respectively.

## References

- Al-Sanad, H., Aggour, M.S. and Yang J.C.S. (1983), "Dynamic shear modulus and damping ratio from random loading tests", *Geotech. Test. J.*, **6**(3), 120-127.
- Auger, F. and Flandrin, P. (1995), "Improving the readability of time-frequency and timescale representations by the reassignment method", *IEEE T. Signal Proces.*, **43**(5), 1068-1089.
- Bagheripour, M.H., Rahgozar, R. and Malekinejad, M. (2010), "Efficient analysis of SSI problems using infinite elements and wavelet theory", *Geomech. Eng.*, **2**(4), 229-252.
- Boltežar, M. and Slavič, J. (2004), "Enhancements to the continuous wavelet transform for damping identification on short signals", *Mech. Syst. Signal Pr.*, **18**(5), 1065-1076.
- Brevdo, E., Fuèkar, N.S., Thakur, G. and Wu, H.T. (2011), "The Synchrosqueezing algorithm: a robust analysis tool for signals with time-varying spectrum", arXiv:1105.0010v1
- Carmona, R.A., Hwang, W.L. and Torresani, B. (1997), "Characterization of signals by the ridges of their wavelet transforms", *IEEE T. Signal Proces.*, **54**(10), 2586-2590.
- Chan, Y.H., Wu, H.T., Hseu, S.S., Kuo, C.T. and Yeh, Y.H. (2011) "ECG-derived respiration and instantaneous frequency based on the synchrosqueezing transform: Application to patients with atrial fibrillation", arXiv: 1105.1571v1
- Chassande-Mottin, E., Auger, F. and Flandrin, P. (2003), "Time-frequency/timescale reassignment", *Wave. Signal Proces.*, 233-267.
- Chassande-Mottin, E., Daubechies, I., Auger, F. and Flandrin, P. (1997), "Differential reassignment", *IEEE Signal Proc. Let.*, **4**(10), 293-294.
- Chen, S.L., Liu, J.J. and Lai, H.C. (2009), "Wavelet analysis for identification of damping ratios and natural frequencies", *J. Sound Vib.*, **323**(1-2), 130-147.
- Cole, H.A. (1968), "On-the-line analysis of random vibrations", *Proceedings of the AIAA/ASME Ninth Structures Structural Dynamics and Materials Conference*, Palm Springs, CA.
- Daubechies, I. and Maes, S. (1996), "A nonlinear squeezing of the continuous wavelet transform based on auditory nerve models", *Wave. Med. Biology*, CRC Press, 527-546.
- Daubechies, I., Lu, J. and Wu, H.T. (2011), "Synchrosqueezed wavelet transforms: An empirical mode decomposition-like tool", *Appl. Comput. Harmon. A.*, **30**(2), 243-261.
- Feldman, M. (2006), "Time varying vibration decomposition and analysis based on the Hilbert transform", *J. Sound Vib.*, **295**(3-5), 518-530.
- Feldman, M. (2011), "Hilbert transform in vibration analysis", *Mech. Syst. Signal Pr.*, **25**(3), 735-802.
- Feldman, M. (2011b), *Hilbert transform applications in mechanical vibrations*, Wiley.
- Gabor, D. (1946), "Theory of communication", *Proceedings of the IEEE 93(III)*.
- Gokdag, H. and Kopmaz, O. (2010), "A new structural damage detection index based on analyzing vibration modes by the wavelet transform", *Struct. Eng. Mech.*, **35**(2), 257-260.

- Grossman, A. and Morlet, J. (1984), "Decomposition of Hardy Functions into square integrable wavelets of constant shape", *SIAM J. Math. Anal.*, **15**(4), 723-736.
- Grossman, A. and Morlet, J. (1990), *Decompositions of functions into wavelets of constant shape and related transforms*, Mathematics and Physics - Lecture on Recent Results, World Scientific, Singapore, 135-65.
- Hahn, S.L. (1996), *Hilbert transforms in signal processing*, Artech House, Boston.
- Hilbert, D. (1953), *Grundzüge einer allgemeinen theorie der linearen integralgleichungen*, Chelsea Pub. Co.
- Huang, N.E. (2005), *Introduction to the Hilbert Huang transform and its related mathematical problems*, Hilbert Huang Transform and Its Applications, World Scientific, 1-26.
- Huang, N.E., Shen, Z., Long, S.R., Wu, M.C., Shih, H.H., Zheng, Q., Yen, N.C., Tung, C.C. and Liu, H.H. (1998), "The empirical mode decomposition and the Hilbert spectrum for nonlinear and non-stationary time series analysis", *Philos. T. R. Soc. A.*, **454**(1971), 903-995.
- Johansson, M. (1999), *The Hilbert transform*, M.S. Thesis, Växjö University.
- Kijewski, T. and Kareem, A. (2003), "Wavelets transform for system identification in civil engineering", *Comput. Aided Civil. Infra. Eng.*, **18**(5), 339-355.
- Korpel, A. (1982), "Gabor: frequency, time, and memory", *Appl. Optics*, **21**(20), 3624-3632.
- Li, C. and Liang, M. (2011), "Time-frequency signal analysis for gearbox fault diagnosis using a generalized synchrosqueezing transform", *Mech. Syst. Signal Pr.*, doi:10.1016/j.ymssp.2011.07.001.
- Montejo, L.A. (2011), "Signal processing based damage detection in structures subjected to random excitations," *Struct. Eng. Mech.*, **40**(6), 745-762.
- Montejo, L.A. and Suarez, L.E. (2006), "Wavelet based identification of site frequencies from earthquake records", *J. Earthq. Eng.*, **10**(3), 565-594
- Rilling, G., Flandrin, P. and Gonçalves, P. (2003), "On empirical mode decomposition and its algorithms", *Proceedings of the IEEEURASIP Workshop on Nonlinear Signal and Image Processing NSIP-03*.
- Slaviè, J., Simonovski, I. and Boltežar, M. (2003), "Damping identification using a continuous wavelet transform: Application to real data", *J. Sound Vib.*, **262**(2), 291-307.
- Staszewski, W.J. (1997), "Identification of damping in MDOF systems using time-scale decomposition", *J. Sound Vib.*, **203**(2), 283-305.
- Thakur, G. and Wu, H.T. (2010), "Synchrosqueezing-based recovery of instantaneous frequency from nonuniform samples", arXiv:1006.2533v3.
- Todorovska, M.I. (2001), *Estimation of instantaneous frequency of signals using the continuous wavelet transform*, Report CE 01-07, Department of Civil Engineering, University of Southern California.
- Ville, J. (1948), "Theorie et application de la notion de signal analytical", *Cables et Transmissions*, **2A**(1), 61-74.
- Wu, H.T. (2011), "Instantaneous frequency and wave shape functions", arXiv:1104.2365v1.
- Wu, Z. and Huang, N.E. (2009), "Ensemble empirical mode decomposition: A noise assisted data analysis method", *Adv. Adaptive Data Anal.*, **1**(1), 1-41.
- Yan, B. and Miyamoto, A. (2006), "A comparative study of modal parameter identification based on wavelet and Hilbert-Huang transforms", *Comput. Aided Civil Infra. Eng.*, **21**(1), 9-23.
- Yang, J.N., Lei, Y., Lin, S. and Huang, N. (2004), "Hilbert-Huang based approach for structural damage detection", *J. Eng. Mech.- ASCE*, **130**(1), 85-95.